2024 IEEE International Conference on Robotics and Automation (ICRA 2024)
May 13-17, 2024. Yokohama, Japan

A Force-driven and Vision-driven Hybrid Control Method of Autonomous Laparoscope-Holding Robot

Jin Fang, *Student Member, IEEE*, Ling Li*, Xiaojian Li, *Member, IEEE*, Hangjie Mo, *Member, IEEE*, Pengxin Guo, Xilin Xiao, Yanwei Qu

***Abstract*—Laparoscope-holding robots significantly enhance the stability and precision of visualization in minimally invasive surgeries. Most existing robots of this kind depend on visual servo systems and struggle with efficient, rapid adjustments in the field-of-view (FOV), especially when identifying organs and needles outside the FOV. This paper presents a laparoscope-holding robot system capable of employing both vision-driven and force-driven mechanisms for continuous and large-scale FOV adjustments, respectively. The system features an integrated tactile handle, enabling the reception of human-robot interaction forces during surgical navigation. We propose a hybrid control method that leverages both force and vision inputs for laparoscopic FOV adjustments. This approach integrates a virtual wrench, generated from visual information, and an interaction wrench, obtained from the tactile handle, into the robot's dynamic model, which complies with remote center of motion constraints. The interaction wrench's gain is adjusted with the gripping force on the integrated tactile handle, ensuring that unintended movements caused by accidental contacts are prevented, thus safeguarding operational safety. The proposed method eliminates the need to switch control modes, enabling simultaneous visual tracking and tactile interaction guidance. Experimental results demonstrate that the proposed method not only allows for FOV adjustments with surgical instrument guiding but also adapts well to large-scale FOV adjustment tasks.**

I. Introduction

As robotics technology increasingly merges with the medical field, medical robots are showing significant promise in enhancing surgical efficiency and precision [1]. In recent years, medical robots have experienced vigorous growth and widespread attention [2]. Among these, laparoscope-holding robot systems stand out as a prime example, attracting considerable attention in both academic and industrial circles [3, 4]. These systems have the potential to optimize the use of high-quality human resources and alleviate the burden on surgeons [5]. Unlike traditional manual methods, laparoscope-holding robots offer surgeons a more accurate and stable field of view (FOV) during laparoscopic procedures, thereby improving the safety and efficiency of minimally invasive surgeries [6].

Most of the laparoscope-holding robot systems used in clinical practice still predominantly rely on surgeon-guided control modes. These control modes can be broadly categorized into two types: powered and unpowered. Unpowered laparoscope-holding robots require manual adjustments by the surgeon and serve primarily to alleviate muscle fatigue. This mode is characterized by cumbersome operation, delayed coordination, and would increase surgical time. Powered laparoscope-holding surgical robots, while eliminating the need for the surgeon to set down surgical instruments to operate the laparoscope, typically require the surgeon to divert their attention during surgery to control the laparoscope. For example, Nishikawa et al. designed a human-machine interface that uses facial movements to control laparoscope motion [7]. Fujii et al. utilized eye movements to guide laparoscope motion [8]. Zhong et al. developed a foot-controlled laparoscope robot system with a clinical learning curve of less than 4 minutes [9]. Sandoval et al. developed an autonomous laparoscope system equipped with exteroceptive sensors to monitor the real-time movement of surgical instruments [10]. It is evident that these methods require surgeons to perform multitasking during surgery, potentially diverting their attention away from critical surgical procedures, and thus may not fully meet clinical requirements.

To enable the surgeon without distraction on adjusting the laparoscopic FOV, visual servo technology has been introduced in this field to achieve autonomous FOV adjustment of laparoscope-holding robot systems [11-14]. In the context of visual servo, the initial phase entails the identification of instruments within the laparoscope image. Subsequently, control algorithms are developed to modify the robot's position and orientation, effectively directing the instruments toward the center of the image. For example, Zhang et al. utilized a multi-objective optimization strategy to achieve position and pose adjustments of laparoscope-holding robots [15]. In recent years, methods that utilize deep learning to learn surgeon's operating behaviors from video and estimate laparoscope motion strategies have also been proposed [16-18]. A multi-instrument tracking vector is proposed by us to prevent regions of interest from moving out of the FOV [19]. During clinical operations, it is commonly observed that surgeons place items such as gauze and needles outside the FOV to prevent them from interfering with ongoing procedures [20]. When these items need to be used again, there is a need for quick FOV switching. Existing visual servo or deep learning prediction methods are based on instrument recognition or detection in the laparoscopic image, while the desired items are not within the image, guidance by instruments alone proves to be inefficient.

This work is fully supported by the National Natural Science Foundation of China (62133004, 72293585 and 72188101), the Anhui Provincial Natural Science Foundation (2108085J33), and the Anhui Provincial Major Science and Technology Project (202203a05020010), the Fundamental Research Funds for the Central Universities (JZ2022HGPA0311 and JZ2023HGQA0125).

J. Fang, L. Li, X. J. Li, H. J. Mo, P. X. Guo, X. L. Xiao, and Y. W. Qu are with the School of Management, Hefei University of Technology, Hefei, China, and the Key Laboratory of Process Optimization and Intelligent Decision-Making (Ministry of Education), Hefei University of Technology, Hefei, China. (Corresponding author: Ling Li; email: cynerelee@hfut.edu.cn)

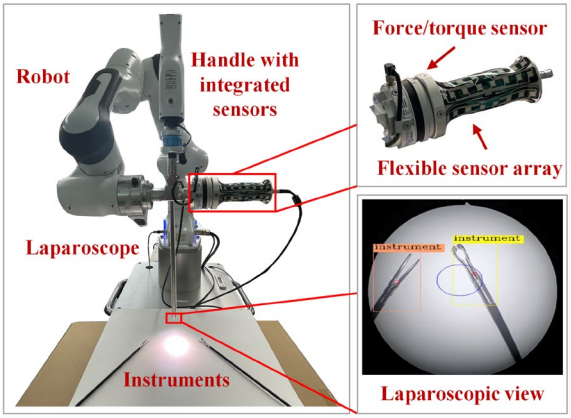

Figure 1. Laparoscope control system.

Therefore, this paper proposed a laparoscope-holding robot system that combines vision-driven continuous FOV adjustment with force-driven large-scale FOV adjustment simultaneously. A laparoscope-holding robot system with an integrated tactile handle has been designed. This system is capable of receiving human-robot interaction forces during surgical area tracking. A hybrid control method for laparoscopic FOV adjustment, which combines both force-driven and vision-driven approaches is proposed. In this method, a virtual wrench generated from visual information and the interaction wrench captured by the integrated tactile handle is simultaneously integrated into the dynamic model of the laparoscope with remote center of motion (RCM) constraints. The gain of the interaction wrench is adjusted in accordance with the gripping force applied to the integrated tactile handle. This gain ensures that any interaction forces resulting from accidental contact do not cause unintended robot movements, thereby enhancing surgical safety. The proposed method eliminates the need to switch between control modes, enabling concurrent visual tracking and tactile interaction guidance. Experimental results validate the method's effectiveness in enabling FOV adjustments guided by surgical instruments and its suitability for large-scale FOV adjustment tasks.

II. LAPAROSCOPE CONTROL SYSTEM

A. System Description

The proposed system comprises a 30° laparoscope, a handle with integrated sensors, and a 7-DoF collaborative robot, as illustrated in Fig. 1. The laparoscope (J1830, Shenyang Shenda Laparoscope Co., Ltd., China) is mounted at the end-effector of the robot and primarily serves to capture visual information about the internal conditions within a patient's body. The YOLO v7 algorithm is employed to detect the positions of surgical instruments within the laparoscopic images, with the detection results being converted into control signals to guide the actions of the robot.

The integrated tactile handle is equipped with both a force/torque sensor (HEX-E-V2, OnRobot, Denmark) and a flexible sensor array (Zhongke Benyuan Information Technology Co., Ltd., China). The force/torque sensor is used to measure the force and torque applied by the surgeon to the laparoscope. The flexible sensor array is employed to measure the tightness of the grip maintained by the surgeon on the handle. The flexible sensor array comprises 64 sensing elements, each initially registering a measurement of 0 in the absence of force. When the surgeon applies force, a value within the range of (0, 255] is recorded, with higher values corresponding to stronger forces applied to the sensing element.

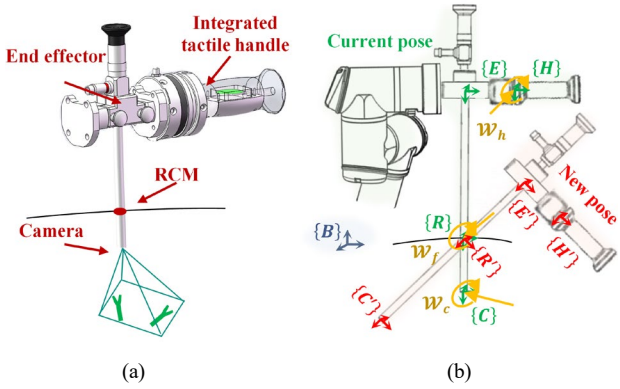

Figure 2. The system setup. (a) Schematic of the laparoscope control system. (b) Frames of the laparoscope control system and wrenches applied to the laparoscope control system.

The collaborative robot used in this system is the 7-dof Franka Emika Robot, developed by Franka Emika GmbH, Germany. In this system, the Franka Emika robot is in the joint velocity control mode of operation.

B. Frames Definition

As depicted in Fig. 2(a), the system involves a laparoscopic robot operating under the constraint of the RCM point. During surgery, it is crucial to avoid applying lateral forces to the incision walls during the manipulation of instruments to prevent injury to the patient. The incision can be regarded as a RCM point, representing a constraint that must be consistently respected throughout the procedure. A force/torque sensor is affixed to the robot's end effector, measuring the force and torque applied by the surgeon. The laparoscope's movement is guided by the robot while adhering to the RCM point constraint. In Fig. 2(b), the reference frames definition is shown. The base frame, $\{B\}$, is regarded as the base frame of the robot. When the robot is in its initial pose, the frames of the laparoscopic system are denoted as $\{*\}$. As the robot undergoes motion, the frames of the laparoscopic system in current are represented as $\{*'\}$. The fulcrum frame, $\{R\}$, is positioned at the incision point when the robot is in its initial pose, with its origin $\boldsymbol{O}_R^B \in \mathbb{R}^3$ in the base frame $\{B\}$ regarded as the RCM point. $\{R'\}$ is the fulcrum frame in the current time and its origin $\boldsymbol{O}_{R'}^B \in \mathbb{R}^3$ is positioned at the RCM point. The robot's end effector frame, denoted as $\{E\}$ and $\{E'\}$, has its origin positioned at the axis of the laparoscope. The transformation between the end effector and the base is $\boldsymbol{T}_E^B(\boldsymbol{q}) \in \mathbb{R}^{4\times4}$, $\boldsymbol{q} \in \mathbb{R}^\lambda$ is the robot's joint positions, where λ signifies the degrees of freedom (DOFs) of the robot. The tactile handle frame is denoted as $\{H\}$ and $\{H'\}$, and the laparoscopic frame is denoted as $\{C\}$ and $\{C'\}$.

C. Overall Framework

The overall system framework, as illustrated in Fig. 3, allows the surgeon to make adjustments to the laparoscopic view either locally or over a larger area. This control is

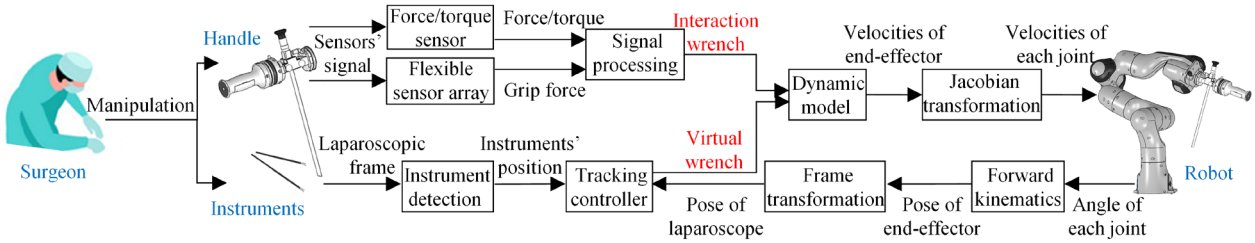

Figure 3. The framework of the proposed laparoscope control system.

achieved by enabling the surgeon to manipulate the laparoscope's movement through two distinct methods: moving the surgical instruments and applying force and torque to the tactile handle. The laparoscope is integrated into the end-effector of a collaborative robot to capture real-time surgical scenes and generate laparoscopic images. These images are then analyzed using the YOLO v7 algorithm to identify the positions of surgical instruments. The detected information is utilized by a tracking controller to produce virtual wrenches. A tactile handle equipped with both force/torque sensors and a flexible sensor array is mounted on the laparoscope. These sensor readings are processed to create interaction wrenches that represent the surgeon's input. A dynamic model combines these two types of wrenches to calculate end-effector velocity. A Jacobian transformation further translates this velocity into joint velocities for the robot. Consequently, the collaborative robot receives these joint velocities as commands to control the laparoscope's motion.

III. Method

This section begins by introducing the laparoscopic dynamic model with the RCM constraint. Subsequently, three types of wrenches are defined as inputs to the laparoscopic dynamic model. Finally, a robot velocity conversion method is presented, where the outputs of the dynamic model are transformed into robot control commands that are applied to the robot.

A. Dynamic Model

The laparoscope is inserted into the patient's body through natural orifices or minor incisions. To prevent the laparoscope from tearing the incision wall, the movement of the laparoscope under the constraint of RCM can be simplified as four DOFs rigid-body motion that consistently passes through a fulcrum point $\boldsymbol{O}_R^B$: three distinct rotations centered around the fulcrum point $\boldsymbol{O}_R^B$ and one translation along the longitudinal axis $\boldsymbol{z}_{R'}$ of the laparoscope. Then the vector representing angular velocity $\dot{\boldsymbol{\varphi}}_{R'}$ and the linear velocity $\dot{\boldsymbol{p}}_{R'}$ of the laparoscope with respect to the current RCM frame $\{R'\}$ writes

$$\begin{bmatrix}\dot{\boldsymbol{\varphi}}_{R'}\\ \dot{\boldsymbol{p}}_{R'}\end{bmatrix}=\begin{bmatrix}\dot{\boldsymbol{\varphi}}_{R'}^{x}+\dot{\boldsymbol{\varphi}}_{R'}^{y}+\dot{\boldsymbol{\varphi}}_{R'}^{z}\\ \boldsymbol{0}+\boldsymbol{0}+\dot{\boldsymbol{p}}_{R'}^{z}\end{bmatrix}=\begin{bmatrix}\dot{\boldsymbol{\varphi}}\\ \dot{\boldsymbol{p}}\end{bmatrix}\begin{bmatrix}\boldsymbol{x}_{R'}\\ \boldsymbol{y}_{R'}\\ \boldsymbol{z}_{R'}\end{bmatrix}, \tag{1}$$

$$\begin{bmatrix}\dot{\boldsymbol{\varphi}}\\ \dot{\boldsymbol{p}}\end{bmatrix}=\begin{bmatrix}\dot{\varphi}_x & \dot{\varphi}_y & \dot{\varphi}_z\\ 0 & 0 & \dot{p}_z\end{bmatrix}. \tag{2}$$

Hence, referring to the Newton-Euler equations, the dynamic equation of the laparoscope in four DOFs can be calculated as:

$$\begin{bmatrix}\sum\boldsymbol{M}\\ \sum F_z\end{bmatrix}=\begin{bmatrix}\boldsymbol{I} & \boldsymbol{0}_{3\times1}\\ \boldsymbol{0}_{1\times3} & m\end{bmatrix}\begin{bmatrix}\ddot{\boldsymbol{\varphi}}\\ \ddot{p}_z\end{bmatrix}+\begin{bmatrix}\boldsymbol{sk}(\dot{\boldsymbol{\varphi}})\cdot\boldsymbol{I}\cdot\dot{\boldsymbol{\varphi}}\\ 0\end{bmatrix}, \tag{3}$$

where $\sum\boldsymbol{M}=[\sum M_x \quad \sum M_y \quad \sum M_z]^T\in\mathbb{R}^3$ represents the summation of the torques exerted on the laparoscope, while $\sum F_z$ signifies the summation of forces applied along the longitudinal axis $\boldsymbol{z}_{R'}$ of the laparoscope.

$$\boldsymbol{I}=\begin{bmatrix}I_x & 0 & 0\\ 0 & I_y & 0\\ 0 & 0 & I_z\end{bmatrix};\ \boldsymbol{sk}(\dot{\boldsymbol{\varphi}})=\begin{bmatrix}0 & -\dot{\varphi}_z & \dot{\varphi}_y\\ \dot{\varphi}_z & 0 & -\dot{\varphi}_x\\ -\dot{\varphi}_y & \dot{\varphi}_x & 0\end{bmatrix}, \tag{4}$$

$$I_x=I_y=\frac{m}{12}\left(3e^2+L^2+12{L_r}^2\right),\ I_z=e^2+{L_r}^2. \tag{5}$$

$\boldsymbol{I}\in\mathbb{R}^{3\times3}$, m is the inertia matrix and mass of the laparoscope, respectively. The laparoscope is considered to be a long cylinder with a base radius of e and a height of L. $L_r=\left\|\boldsymbol{O}_R^B-\boldsymbol{O}_{E'}^B\right\|\in[0,L]$ represents the length of the laparoscopic portion outside the body. The $\boldsymbol{sk}(\dot{\boldsymbol{\varphi}})$ is the skew-symmetric matrix associated with the vector $\dot{\boldsymbol{\varphi}}$.

B. Wrenches Definition

As depicted in Fig. 2(b), three wrenches interaction wrench, virtual wrench, and viscous resistance wrench are proposed to control laparoscopic FOV adjustment during the cooperation.

The interaction wrench is determined by the surgeon-operated wrench on the force/torque sensor and the grip force from the flexible sensor array. The interaction wrench incorporates a parameter-adaptive adjustment mechanism to prevent any inadvertent touches or contact.

The surgeon-operated wrench acting on the force/torque sensor is represented by

$$\boldsymbol{\mathcal{W}}_s=\begin{bmatrix}\boldsymbol{M}_s\\ \boldsymbol{F}_s\end{bmatrix}\begin{bmatrix}\boldsymbol{x}_{H'}\\ \boldsymbol{y}_{H'}\\ \boldsymbol{z}_{H'}\end{bmatrix}=\begin{bmatrix}M_s^x & M_s^y & M_s^z\\ F_s^x & F_s^y & F_s^z\end{bmatrix}\begin{bmatrix}\boldsymbol{x}_{H'}\\ \boldsymbol{y}_{H'}\\ \boldsymbol{z}_{H'}\end{bmatrix}, \tag{6}$$

where $\boldsymbol{\mathcal{W}}_s$ is the surgeon-operated wrench, $\boldsymbol{M}_s\in\mathbb{R}^3$ and $\boldsymbol{F}_s\in\mathbb{R}^3$ are the readings of the force/torque sensor. $\boldsymbol{x}_{H'}$, $\boldsymbol{y}_{H'}$, and $\boldsymbol{z}_{H'}$ are the three coordinate axes of the current handle frame $\{H'\}$ with respect to the current RCM frame $\{R'\}$.

Due to the RCM constraint, the movement of the laparoscope is restricted to four DOFs. $\boldsymbol{\mathcal{W}}_h=[\boldsymbol{M}_h \quad \boldsymbol{F}_h]^T[\boldsymbol{x}_{H'} \quad \boldsymbol{y}_{H'} \quad \boldsymbol{z}_{H'}]^T$ can be computed as follows:

$$\boldsymbol{\mathcal{W}}_h=\delta\begin{bmatrix}F_s^y L_r+M_s^x & F_s^x L_r+M_s^y & M_s^z\\ 0 & 0 & F_s^z\end{bmatrix}\begin{bmatrix}\boldsymbol{x}_{H'}\\ \boldsymbol{y}_{H'}\\ \boldsymbol{z}_{H'}\end{bmatrix}, \tag{7}$$

where $\boldsymbol{\mathcal{W}}_h$ is the interaction wrench. $\boldsymbol{M}_h\in\mathbb{R}^3$, and $\boldsymbol{F}_h\in\mathbb{R}^3$ are torques and forces of the interaction wrench.

δ is the gain of the interaction wrench, and:

$$\delta = \begin{cases} 0 & n_c \le k_{min} \\ \ln\left(\frac{\sum_{j=1}^{64} Se_j}{k_H} + 1\right) & k_{min} < n_c \end{cases}, \tag{8}$$

where Se_j represents the measurement value of the j-th sensing element. k_H is a constant that constrains δ within a reasonable range. n_c signifies the number of sensing elements subjected to contact force, while k_{min} represents the minimum number of sensing elements on which contact force needs to be applied to initiate control over the laparoscope. The adaptive adjustment mechanism ensures that control is only initiated when sufficient contact is made, potentially reducing the risk of unintended movements or actions.

The virtual wrench denoted as $\boldsymbol{\mathcal{W}}_c$ is used to prevent instruments from moving out of the FOV. $\boldsymbol{\mathcal{W}}_c = [\boldsymbol{M}_c \quad \boldsymbol{F}_c]^T[\boldsymbol{x}_{C'} \quad \boldsymbol{y}_{C'} \quad \boldsymbol{z}_{C'}]^T$ is computed as follows:

$$\boldsymbol{\mathcal{W}}_c = \begin{cases} \begin{bmatrix} 0 & 0 & 0 \\ 0 & 0 & 0 \end{bmatrix} \begin{bmatrix} \boldsymbol{x}_{C'} \\ \boldsymbol{y}_{C'} \\ \boldsymbol{z}_{C'} \end{bmatrix} & n_s = 0 \\ (L - L_r) \begin{bmatrix} \sum_{i=1}^{n_{si}} F_i^y & \sum_{i=1}^{n_{si}} F_i^x & 0 \\ 0 & 0 & 0 \end{bmatrix} \begin{bmatrix} \boldsymbol{x}_{C'} \\ \boldsymbol{y}_{C'} \\ \boldsymbol{z}_{C'} \end{bmatrix} & n_s > 0 \end{cases} \tag{9}$$

where $\boldsymbol{M}_c \in \mathbb{R}^3$ and $\boldsymbol{F}_c \in \mathbb{R}^3$ are torques and forces of the virtual wrench. $\boldsymbol{x}_{C'}$, $\boldsymbol{y}_{C'}$, and $\boldsymbol{z}_{C'}$ are the three coordinate axes of the current laparoscopic frame $\{C'\}$ with respect to the current RCM frame $\{R'\}$; n_s denotes the number of surgical instruments in the image; The visual tracking force $\boldsymbol{F}_i = \begin{bmatrix} F_i^x & F_i^y & F_i^z \end{bmatrix} \in \mathbb{R}^3$ that track $\boldsymbol{\mathcal{P}}_i$ designed in our previously published paper [19], and $\boldsymbol{F}_i$ is expressed as:

$$\boldsymbol{F}_i = F(d_i) \cdot \boldsymbol{V}_i, \tag{10}$$

d_i, $F(d_i)$, and $\boldsymbol{V}_i$ are computed as follows:

$$d_i = \sqrt{u_i^2 + v_i^2}, \tag{11}$$

$$F(d_i) = \begin{cases} 0 & d_i \le r \\ \frac{F_{max}}{2}\left(\sin\frac{(d_i - r)\pi}{2(R - d_i)} + 1\right) & r < d_i \le R, \\ F_{max} & R < d_i \end{cases} \tag{12}$$

$$\boldsymbol{V}_i = \frac{\boldsymbol{z}_{C'} \times \boldsymbol{\mathcal{P}}_i' \times \boldsymbol{\mathcal{P}}_i'}{\left\| \boldsymbol{z}_{C'} \times \boldsymbol{\mathcal{P}}_i' \times \boldsymbol{\mathcal{P}}_i' \right\|} \tag{13}$$

where $\boldsymbol{V}_i$ represents the unit direction in which the laparoscope needs to move to track $\boldsymbol{p}_i$. $\boldsymbol{\mathcal{P}}_i' \in \mathbb{R}^3$ represents the position of the surgical instrument scaled to the unit depth in the laparoscopic frame, which can be expressed as follows:

$$\boldsymbol{\mathcal{P}}_i' = \left[\frac{u_i - u_0}{f_x} \cdot \boldsymbol{x}_{C'} \quad \frac{v_i - v_0}{f_y} \cdot \boldsymbol{y}_{C'} \; \boldsymbol{z}_{C'} \right]^T, \tag{14}$$

f_x, f_y, u_0 and v_0 are the camera parameters. $d_i \in \left[0, \sqrt{u_0^2 + v_0^2}\right]$ represents the distance between the $\boldsymbol{p}_i$ and the image center; The function $F(d_i) \in [0, F_{max}]$ demonstrates continuity and differentiability across its domain, where F_{max} represents the maximum force that can be achieved when tracking $\boldsymbol{p}_i$.

The viscous resistance wrench $\boldsymbol{\mathcal{W}}_f$ is proposed to ensure system stability. It incorporates the application of viscous resistance to control the four DOFs movement of the laparoscope.

$$\boldsymbol{\mathcal{W}}_f = \begin{bmatrix} \boldsymbol{M}_f \\ \boldsymbol{F}_f \end{bmatrix} = -\begin{bmatrix} k_f\dot{\varphi}_x & k_f\dot{\varphi}_y & k_f\dot{\varphi}_z \\ 0 & 0 & k_t\dot{p}_z \end{bmatrix} \begin{bmatrix} \boldsymbol{x}_{R'} \\ \boldsymbol{y}_{R'} \\ \boldsymbol{z}_{R'} \end{bmatrix}, \tag{15}$$

where $\boldsymbol{M}_f \in \mathbb{R}^3$ and $\boldsymbol{F}_f \in \mathbb{R}^3$ are torques and forces of the viscous resistance wrench. k_f and k_t are positive viscous resistance parameters. $\boldsymbol{x}_{R'}$, $\boldsymbol{y}_{R'}$, and $\boldsymbol{z}_{R'}$ are the three coordinate axes of the RCM frame $\{R'\}$.

Due to the frames on the laparoscope being rigidly transformed and do not involve inter-rotation, it can be derived that

$$\begin{bmatrix} \boldsymbol{x}_{H'} \\ \boldsymbol{y}_{H'} \\ \boldsymbol{z}_{H'} \end{bmatrix} = \begin{bmatrix} \boldsymbol{x}_{C'} \\ \boldsymbol{y}_{C'} \\ \boldsymbol{z}_{C'} \end{bmatrix} = \begin{bmatrix} \boldsymbol{x}_{R'} \\ \boldsymbol{y}_{R'} \\ \boldsymbol{z}_{R'} \end{bmatrix}. \tag{16}$$

Consequently, $[\sum \boldsymbol{M} \quad \sum F_z]^T$ can be computed as follows:

$$\begin{bmatrix} \sum \boldsymbol{M} \\ \sum F_z \end{bmatrix} = \begin{bmatrix} \boldsymbol{M}_h + \boldsymbol{M}_c + \boldsymbol{M}_f \\ F_h^z + F_c^z + F_f^z \end{bmatrix}. \tag{17}$$

C. Robot Velocity Conversion

To avoid gimbal lock issues, the angular acceleration $\ddot{\boldsymbol{\varphi}}$ of the laparoscope is transformed into quaternion velocity $\dot{\boldsymbol{Q}} \in \mathbb{R}^4$.

$$\dot{\boldsymbol{Q}} = [0 \quad \ddot{\varphi}_x \cdot \Delta t \quad \ddot{\varphi}_y \cdot \Delta t \quad \ddot{\varphi}_z \cdot \Delta t]^T, \tag{18}$$

where Δt represents the differential of time.

With respect to frame $\{R\}$, the new posture of the laparoscope, represented by quaternions, $\boldsymbol{Q}_N \in \mathbb{R}^4$ can be calculated as follows:

$$\boldsymbol{Q}_N = \boldsymbol{Q}_O + \frac{1}{2} \cdot Qm(\boldsymbol{Q}_O, \dot{\boldsymbol{Q}}) \cdot \Delta t, \tag{19}$$

where $\boldsymbol{Q}_O \in \mathbb{R}^4$ represents the quaternion form of the laparoscope rotation $\boldsymbol{\mathcal{R}}_{R'}^R \in \mathbb{R}^{3\times3}$, $\boldsymbol{\mathcal{R}}_{R'}^R$ is the rotation part of $\boldsymbol{T}_{R'}^R \in \mathbb{R}^{4\times4}$. $Qm(\cdot)$ denotes quaternion multiplication.

The translation $\boldsymbol{t}_N \in \mathbb{R}^3$ of the laparoscope with respect to the frame $\{R\}$ can be calculated as follows:

$$\boldsymbol{t}_N = \boldsymbol{t}_O + \boldsymbol{\mathcal{R}}_{R'}^R \begin{bmatrix} 0 \\ 0 \\ L - L_r + \dot{p}_z \cdot \Delta t + \ddot{p}_z \cdot (\Delta t)^2 \end{bmatrix}, \tag{20}$$

where $\boldsymbol{t}_O \in \mathbb{R}^3$ represents the translation part of $\boldsymbol{T}_{R'}^R$.

Therefore, the new pose of the laparoscope $\boldsymbol{T}_{R_N'}^R \in \mathbb{R}^{4\times4}$ with respect to $\{R\}$ can be calculated as follows:

$$\boldsymbol{T}_{R_N'}^R = \begin{bmatrix} Qt\mathcal{R}(\boldsymbol{Q}_N) & \boldsymbol{t}_N \\ \boldsymbol{0} & 1 \end{bmatrix}, \tag{21}$$

where $Qt\mathcal{R}(\cdot)$ is a function that converts quaternions into a rotation matrix.

After the frame transformation, the transformation between the current and new robot's end effector frame $\{E_N'\}$ and $\{E'\}$ with respect to the frame $\{B\}$ can be calculated as:

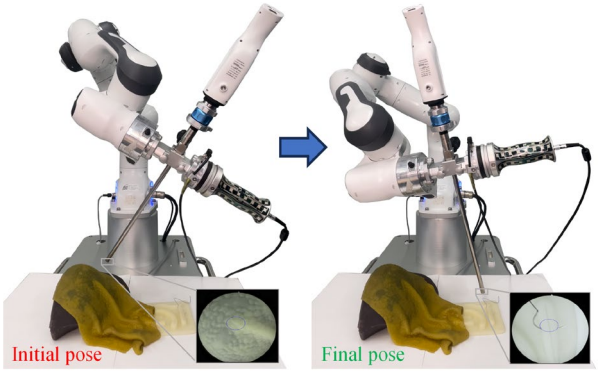

Figure 4. Completing the laparoscope FOV adjustment task using grips of varying strengths. Experimental scenario: initial pose (left), final pose (right).

$$\boldsymbol{T}_{E_N'}^{B} = \boldsymbol{T}_{E}^{B} \cdot \boldsymbol{T}_{R}^{E} \cdot \boldsymbol{T}_{R_N'}^{R} \cdot \boldsymbol{T}_{E_N'}^{R_N'}, \tag{22}$$

$$\boldsymbol{T}_{E'}^{B} = \boldsymbol{T}_{E}^{B} \cdot \boldsymbol{T}_{R}^{E} \cdot \boldsymbol{T}_{R'}^{R} \cdot \boldsymbol{T}_{E'}^{R'}, \tag{23}$$

where $\boldsymbol{T}_{E}^{B} \in \mathbb{R}^{4\times4}$ is a fixed frame transformation that is recorded at the initial state of the robot. As the laparoscope remains a rigid body, the transformation relationship between frame $\{E\}$ and $\{R\}$ remains constant, which implies $(\boldsymbol{T}_{R}^{E})^{-1} = \boldsymbol{T}_{E'}^{R'} = \boldsymbol{T}_{E_N'}^{R_N'} \in \mathbb{R}^{4\times4}$.

By applying real-time Jacobian transformation, the robot's joint space velocity $\dot{\boldsymbol{q}}_{\boldsymbol{N}} \in \mathbb{R}^{\lambda}$ can be calculated as follows:

$$\dot{\boldsymbol{q}}_{\boldsymbol{N}} = \mathcal{J}\left(\boldsymbol{T}_{E_N'}^{B}, \boldsymbol{T}_{E'}^{B}\right), \tag{24}$$

where $\mathcal{J}(\cdot)$ represents the real-time Jacobian transformation relationship of the robot.

IV. Experiment

To validate the proposed system's effectiveness, experiments were conducted using the platform shown in Fig. 1. The RCM point is set on the axis of the laparoscope, and by performing fixed frame transformation $\boldsymbol{T}_{R}^{E}$ on the initial end effector posture $\boldsymbol{T}_{E}^{B}$, the initial posture of the RCM frame $\boldsymbol{T}_{R}^{B}$ can be determined. The model is integrated every 1 ms using the Euler method in order to generate the reference joint positions to be provided to the robot. High tracking accuracy is expected with this Franka operation control mode.

The laparoscopic system is attached at the end effector of the robot which communicates with the computer through a USB port. The frame rate is set at 25 fps. The laparoscope calibration method proposed by Zhang et al. [21] was used to calibrate the intrinsic parameters of a laparoscope. The YOLO v7 algorithm was employed to achieve high-performance, low-latency surgical instrument detection.

A. Parameter setting

During the experiments, the laparoscope's mass, denoted as m, is set to 1 kg. The laparoscope is considered to be a slender cylinder with a radius e of 0.01 m and a height L of 0.2951 m. The initial length of the laparoscope outside the body L_r, is set to 0.1 m. The intrinsic camera parameters for the laparoscopic camera are defined as: $u_0 = 312.221$, $v_0 = 243.391$, $f_x = 506.565$, and $f_y = 506.719$. The tracking distance boundaries are set as $r = 20$ pixels and $R = 200$ pixels, respectively. The maximum tracking force is set as $F_{max} = 100N$. The parameters for the flexible force-sensitive sensor are configured with a value of 2000 for k_H and 3 for k_{min}. The parameter for viscous resistance, k_f, is specified as 2, and k_t is set to 150.

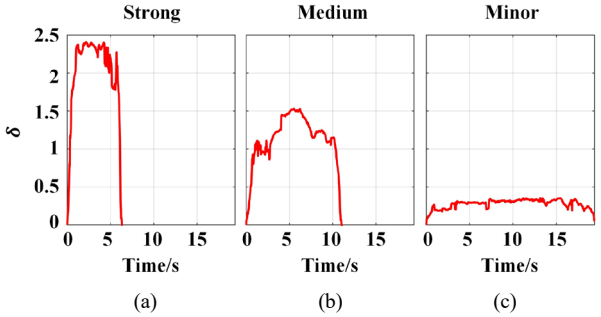

Figure 5. The values of δ in the three experiments: (a) Strong force. (b) Medium force. (c) Minor force.

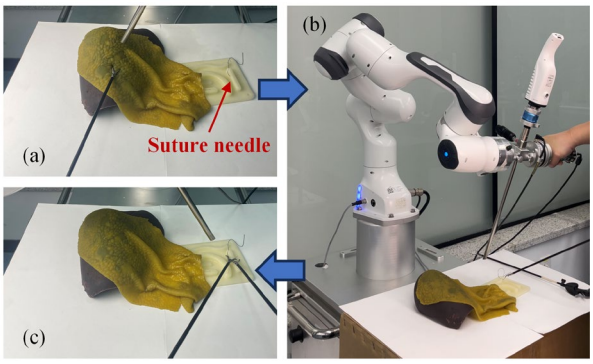

Figure 6. Experimental scenario for suture needle search: (a) Image-based surgical instrument tracking in a localized region. (b) Laparoscopic large-scale FOV adjustment controlled by handle and search for suture needle. (c) Retrieve the suture needle.

B. Impact of δ on tracking performance

This experiment aimed to assess the laparoscope system compliance when applying various grip forces to the flexible sensor array. The laparoscope system compliance was quantified by analyzing the time required to achieve equivalent adjustments in the laparoscopic view. The experimental setup is illustrated in Fig. 4.

The value of δ is used to assess the magnitude of grip force applied by the operator. The greater the grip force, the larger the value of δ. As shown in Fig. 5, when the operator applied three different levels of grip force to the handle, ranging from strong to minor, the average values of δ were 2.01, 1.13, and 0.28, respectively. The time taken to complete the same laparoscopic view adjustments were 6.32 seconds, 11.0 seconds, and 19.46 seconds, respectively. The experimental results suggest that the operator applies a stronger grip force to the handle, resulting in a shorter time required for laparoscopic adjustments. The design of this mechanism aims to ensure that the laparoscope does not move when the surgeon unintentionally comes into contact with the handle.

C. Searching for a suture needle

In minimally invasive surgery, the limited FOV requires

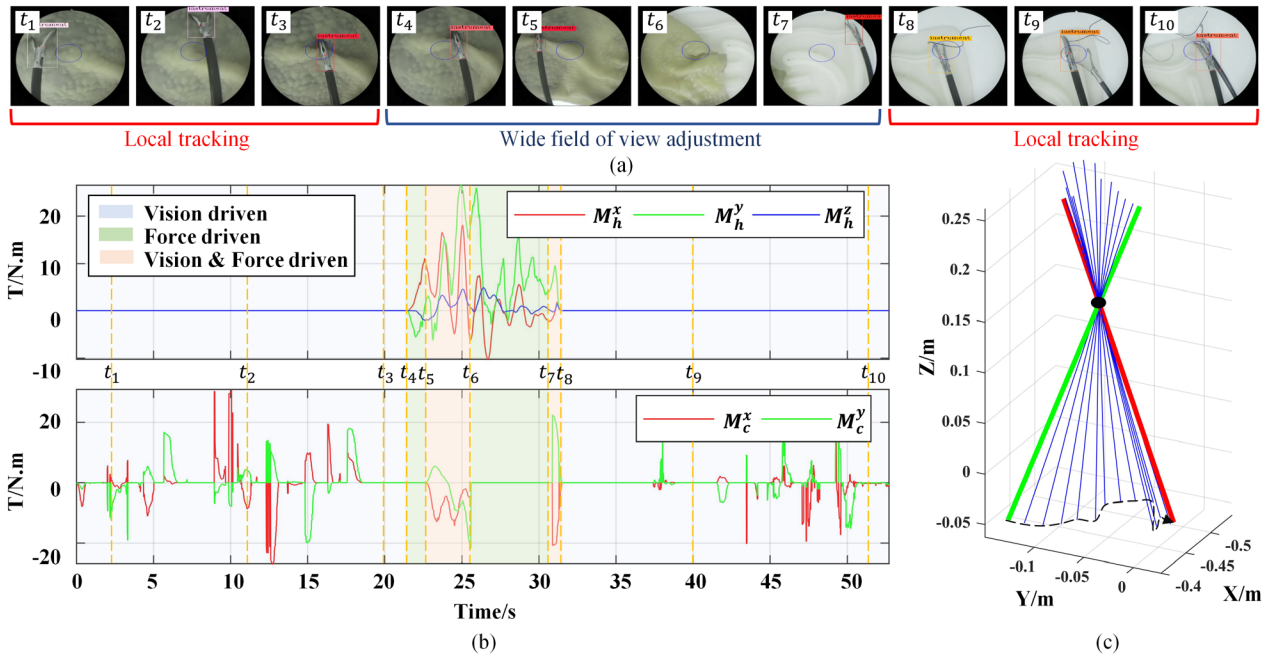

Figure 7. Experimental results for suture needle searching. (a) The experimental snapshots. (b) Wrenches were applied in the laparoscope. (c) Traces of the laparoscope axis: initial pose (green line), final pose (red line), fulcrum (black dot), trajectory of the laparoscope's distal end (black dashed arrow).

surgeons to make substantial laparoscope adjustments to locate suture needles beyond their current visual range. In this experiment, the operator aims to find a suture needle placed on simulated organs, as depicted in Fig. 6. Initially, the operator maneuvers surgical instruments within a localized area. Subsequently, the operator manipulates the tactile handle to facilitate large-scale FOV adjustments, locating the suture needle.

Figure 7 illustrates the experimental results: (a) shows a snapshot with the laparoscope's tracking boundary marked by a blue circle of 20 pixels radius; (b) displays the interaction wrench $\boldsymbol{\mathcal{W}_h}$ and the virtual wrench $\boldsymbol{\mathcal{W}_c}$; and (c) details the laparoscope axis traces, these results affirm that the laparoscope's movement consistently adhered to the RCM constraints throughout the experiment.

In the initial phase, the operator manipulates the surgical instrument on the artificial organ, generating the virtual wrench $\boldsymbol{\mathcal{W}_c}$ to track the instrument's motion from time 0 to t_3. At t_4, the instrument ceases movement, maintaining its position within the screen's central region. Following this, the operator applies the interaction wrench $\boldsymbol{\mathcal{W}_h}$ to the tactile handle, initiating control over the laparoscope to locate the suture needle.

At time t_5, the interaction wrench $\boldsymbol{\mathcal{W}_h}$ exceeds the virtual wrench $\boldsymbol{\mathcal{W}_c}$, causing a deviation of the laparoscope from the current viewpoint. After t_6, the instrument becomes invisible in the image. Subsequently, the operator significantly adjusts the FOV to accurately locate the suture needle.

By time t_7, the suture needle appears at the edge of the screen. At this juncture, upon the operator releasing the tactile handle, a virtual wrench $\boldsymbol{\mathcal{W}_c}$ is generated, facilitating the rapid repositioning of the surgical instrument back to the center of the screen. Subsequently, from t_8 to t_{10}, with the assistance of laparoscopic tracking, the operator successfully retrieves the suturing needle.

V. Conclusion

This paper presents a novel laparoscope-holding robot system featuring an integrated tactile handle for enhanced human-robot interaction during surgical area tracking. We propose a hybrid control method that merges force-driven and vision-driven approaches for precise FOV adjustments. This method eliminates the need to switch between control modes, facilitating simultaneous visual tracking and tactile interaction. Experimental results validate that this approach not only supports FOV adjustments with surgical instrument guidance but also accommodates large-scale FOV modifications. In future work, we plan to refine the dynamic model to include considerations for dynamic RCM constraints, aiming to offset the impact of dynamic variations in RCM positioning due to factors such as patient respiration and organ movement.

References

[1] A. M. Okamura, M. J. Matarić, and H. I. Christensen, "Medical and health-care robotics," *IEEE Robotics & Automation Magazine,* vol. 17, no. 3, pp. 26-37, 2010.

[2] R. H. Taylor, A. Menciassi, G. Fichtinger, P. Fiorini, and P. Dario, "Medical robotics and computer-integrated surgery," *Springer handbook of robotics,* pp. 1657-1684, 2016.

[3] R. Polet and J. Donnez, "Using a laparoscope manipulator (LAPMAN) in laparoscopic gynecological surgery," *Surg Technol Int,* vol. 17, no. 187, p. 45, 2008.

[4] C. Bergeles and G.-Z. Yang, "From passive tool holders to microsurgeons: safer, smaller, smarter surgical robots," *IEEE Transactions on Biomedical Engineering,* vol. 61, no. 5, pp. 1565-1576, 2013.

[5] B. Yang *et al.*, "Adaptive fov control of laparoscopes with programmable composed constraints," *IEEE Transactions on Medical Robotics and Bionics,* vol. 1, no. 4, pp. 206-217, 2019.
[6] T. Cheng, W. Li, C. S. H. Ng, P. W. Y. Chiu, and Z. Li, "Visual servo control of a novel magnetic actuated endoscope for uniportal video-assisted thoracic surgery," *IEEE Robotics and Automation Letters,* vol. 4, no. 3, pp. 3098-3105, 2019.
[7] A. Nishikawa *et al.*, "FAce MOUSe: A novel human-machine interface for controlling the position of a laparoscope," *IEEE Transactions on Robotics and Automation,* vol. 19, no. 5, pp. 825-841, 2003.
[8] K. Fujii, G. Gras, A. Salerno, and G.-Z. Yang, "Gaze gesture based human robot interaction for laparoscopic surgery," *Medical image analysis,* vol. 44, pp. 196-214, 2018.
[9] F. Zhong *et al.*, "Foot-controlled robot-enabled endoscope manipulator (freedom) for sinus surgery: Design, control, and evaluation," *IEEE Transactions on Biomedical Engineering,* vol. 67, no. 6, pp. 1530-1541, 2019.
[10] J. Sandoval, M. A. Laribi, J.-P. Faure, C. Breque, J.-P. Richer, and S. Zeghloul, "Towards an autonomous robot-assistant for laparoscopy using exteroceptive sensors: Feasibility study and implementation," *IEEE Robotics and Automation Letters,* vol. 6, no. 4, pp. 6473-6480, 2021.
[11] X. Zhang, W. Li, P. W. Y. Chiu, and Z. Li, "A novel flexible robotic endoscope with constrained tendon-driven continuum mechanism," *IEEE Robotics and Automation Letters,* vol. 5, no. 2, pp. 1366-1372, 2020.
[12] Y. Wang, Q. Sun, Z. Liu, and L. Gu, "Visual detection and tracking algorithms for minimally invasive surgical instruments: A comprehensive review of the state-of-the-art," *Robotics and Autonomous Systems,* vol. 149, p. 103945, 2022.
[13] J. Peng, C. Zhang, L. Kang, and G. Feng, "Endoscope FOV Autonomous Tracking Method for Robot-Assisted Surgery Considering Pose Control, Hand–Eye Coordination, and Image Definition," *IEEE Transactions on Instrumentation and Measurement,* vol. 71, pp. 1-16, 2022.
[14] X. Ma, C. Song, P. W. Chiu, and Z. Li, "Visual servo of a 6-DOF robotic stereo flexible endoscope based on da Vinci Research Kit (dVRK) system," *IEEE Robotics and Automation Letters,* vol. 5, no. 2, pp. 820-827, 2020.
[15] C. Zhang, W. Zhu, J. Peng, Y. Han, and W. Liu, "Visual servo control of endoscope-holding robot based on multi-objective optimization: System modeling and instrument tracking," *Measurement,* vol. 211, p. 112658, 2023.
[16] B. Li, B. Lu, Y. Lu, Q. Dou, and Y.-H. Liu, "Data-driven holistic framework for automated laparoscope optimal view control with learning-based depth perception," in *2021 IEEE International Conference on Robotics and Automation (ICRA)*, 2021: IEEE, pp. 12366-12372.
[17] B. Li, B. Lu, Z. Wang, F. Zhong, Q. Dou, and Y.-H. Liu, "Learning laparoscope actions via video features for proactive robotic field-of-view control," *IEEE Robotics and Automation Letters,* vol. 7, no. 3, pp. 6653-6660, 2022.
[18] J. Zhang *et al.*, "Automatic Keyframe Detection for Critical Actions from the Experience of Expert Surgeons," in *2022 IEEE/RSJ International Conference on Intelligent Robots and Systems (IROS)*, 2022: IEEE, pp. 8049-8056.
[19] L. Li, X. Li, B. Ouyang, S. Ding, S. Yang, and Y. Qu, "Autonomous multiple instruments tracking for robot-assisted laparoscopic surgery with visual tracking space vector method," *IEEE/ASME Transactions on Mechatronics,* vol. 27, no. 2, pp. 733-743, 2021.
[20] G. Fried, A. Derossis, J. Bothwell, and H. Sigman, "Comparison of laparoscopic performance in vivo with performance measured in a laparoscopic simulator," *Surgical endoscopy,* vol. 13, pp. 1077-1081, 1999.
[21] Z. Zhang, "A flexible new technique for camera calibration," *IEEE Transactions on pattern analysis and machine intelligence,* vol. 22, no. 11, pp. 1330-1334, 2000.